Effects of duration of solution heat treatment on the evolution of 3D microstructure in AlSi7Cu3 alloy: A quantitative X-ray tomography study

Zaidao Li, Nathalie Limodin, Amina Tandjaoui, Philippe Quaegebeur, David Balloy

Effects of duration of solution heat treatment on the evolution of 3D microstructure in AlSi7Cu3 alloy: a quantitative X-ray tomography study

Zaidao Li [a,b,*], Nathalie Limodin [a], Amina Tandjaoui [a], Philippe Quaegebeur [a], David Balloy [b]

[a] Univ. Lille, CNRS, Centrale Lille, UMR 9013 - LaMcube – Laboratoire de mécanique multiphysique et multiéchelle, F-59000 Lille, France

[b] Univ. Lille, CNRS, INRA, ENSCL, UMR 8207 - UMET - Unité Matériaux et Transformations, F-59000 Lille, France

Abstract: The evolution of the microstructure of an AlSi7Cu3 alloy is investigated by optical microscopy and X-ray tomography in as-cast condition and with subsequent solution treatments for 2 h 30 min and 50 h at 495 °C, respectively. The analyzed microstructure contains pores and hard inclusions, i.e. eutectic Si, iron-intermetallics, and Al_2Cu phases. 2D microscopic surface examination was performed to reveal the characteristics of eutectic Si phase while 3D characterization by X-ray tomography (Lab-CT) was performed for the pores, iron-intermetallics, and Al_2Cu phases. The 3D quantitative characterization can provide new insight into the microstructures amount, size and morphology change mechanisms during heat treatment. The Al_2Cu phase, which presents a 3D interconnected structure in the as-cast condition, undergoes significant morphological changes during the solution heat treatment. The incipient melting of Al_2Cu phase was evidenced after 50 h of solution treatment at 495°C, which leads to the formation of small pores (<60µm). Statistical analyses of the Al_2Cu particle distribution, their size and their local mean curvatures describe the disintegration of the interconnected network structure followed by the dissolving of the disconnected particles. The eutectic Si undergoes fragmentation, spheroidization, and coarsening during the solution treatment.

Keywords: A319, heat treatment, X-ray tomography, microstructure, 3D characterization

1 Introduction

Al-Si aluminum alloys are now extensively used in various automotive components such as wheels and cylinder heads due to their light weight, good casting characteristics and mechanical properties [1]. The microstructure of Al-Si-Cu alloys can widely affect the mechanical properties, damage mechanisms and the fatigue failure [2,3]. Among the various microstructural parameters to consider are the Secondary Dendrite Arm Spacing (SDAS) [4], as well as the eutectic Si particles size and morphology [5]. Moreover, the amount and morphology of iron-intermetallics [6,7] and Al_2Cu phase [8] are also to be considered. In order to further improve the mechanical properties, as-cast Al-Si-Cu alloys can be heat treated to increase strength through precipitation hardening [9]. The heat treatment consists of solution treatment and quenching followed by artificial aging. The purpose of the solution heat treatment is to: (1) dissolve Cu containing particles formed during solidification; (2) homogenize the alloying elements in solid solution; (3) spheroidize the eutectic Si particles [10]. In order to avoid local melting during solution treatment, the solution temperature of Al-Si-Cu alloy such as the A319 alloy used for cylinder heads is generally restricted below 495 °C [11].

Microstructural changes occur during solution heat treatment. The eutectic Si particles, which have plate-like shape in unmodified alloys, spheroidize [12]: Si particles first fragment, spheroidize and then coarsen [10]. Phases containing Fe are harder to dissolve. Narayanan et al. [13] reported the iron-intermetallics of A1-Si-Cu alloys do not undergo any change when solution temperatures are below the final solidification point. However, high-temperature solution treatment (i.e. 870K) may foster micro pores growth due to incipient local melting [14]. Andilab et al. [15] suggested that incipient melting of Al_2Cu lead to the formation of micro pores in a novel Al-Cu alloy. Dissolution of the Al_2Cu phases takes place at temperatures near the final solidification temperature of the Al-Si-Cu alloy (i.e. 480 °C), and it accelerates with an increase of solution treatment temperature [8]. The dissolution of blocky Al_2Cu phase particles is more difficult than that of fine Al_2Cu phase particles because the blocky Al_2Cu particles do not fragment but dissolve by spheroidization and diffusion, which takes a longer time [16]. Yet, Vandersluis et al. [17] demonstrated the dissolution mechanism during heat treatment for the B319 Al alloy through in-situ 2D characterization techniques, and concluded that both Al_2Cu and $Al_5Mg_8Cu_2Si_6$ phases dissolve synchronously during heat treatment. However, as both the blocky and eutectic Al_2Cu particles form a complex and interconnected network in 3D [18], their dissolution mechanism at a local scale is still unclear.

The morphology and size of these microstructures changes of the Al-Si-Cu alloy after heat treatments have been mainly studied using conventional 2D characterization [16,19,20]. Yet, 2D analyses can be misleading to some extent. For example, the β-Al_5FeSi phase appears as needles in 2D cross section, whilst it appears as a network platelets in 3D [21]. Puncreobutr et al. [22] highlighted the benefits of 3D imaging when comparing with the 2D analysis of an A319 sample. 3D measurements provide more

representative information of microstructures than 2D measurements, and allow obtaining new insights into microstructural evolution within a given phase during heat treatment. X-ray Computed Tomography (CT) is a non-destructive technique to visualize internal 3D geometry of an opaque solid object in order to obtain digital information of the internal structure at a microscopic level [23]. Recently, Zhao et al. [24] demonstrated the effect of ultrasonic melt processing (USP) on the 3D morphologies and distributions of the intermetallic phases (i.e. Fe-rich phases and Al_2Cu) changes in Al-Cu alloys using synchrotron X-ray tomography. Kim et al. [25] studied the 3D morphologies of iron-intermetallics in as-cast and as-rolled Al-Si-Mg-Fe alloys by means of x-ray tomography. Hence X-ray computed tomography has proved to be a powerful technique for providing a proper and accurate quantitative analysis of 3D structures. However, this technique has some limitations: access to synchrotron X-ray tomography is limited due to its high expense [26] and limited availability of the facilities, while Laboratory X-ray tomography cannot be used for low attenuating materials (polymers) or materials containing heterogeneities with similar attenuation coefficients (e.g. Al/Si alloys) [27].

The aim of this paper is to present a detailed microstructural evolution analysis of an A319 aluminum alloy during various solution heat treatments. A full metallographic 2D and 3D characterization of the microstructure through Optical Microscopy (OM) and laboratory X-ray tomography were performed in order to characterize microstructural changes with the variation of solution heat treatment time and also to identify the dissolution mechanisms acting at a local scale.

2 Experimental procedures

2.1 Material and heat treatment

The material used in this work was a Lost Foam Cast A319 alloy with SDAS 75-80 μm, the chemical composition is given in Table 1. Its microstructure commonly consists of α-Al, eutectic Si, Al_2Cu phase, iron-intermetallics and pores.

Table 1: Chemical composition of the experimental A319 alloy (wt. %)

Al	**Si**	**Cu**	**Fe**	**Mn**	**Sr**	**Mg**	**Ti**	**Ni**	**Pb**	**Zn**	**Sn**	**Zr,V,P,Sr**	
												each	total
bal.	7.85	3.05	0.30	0.190	0.0120	0.28	0.098	0.018	<0.015	0.16	<0.015	≤0.03	≤0.1

In this work, small sized dog-bone shape samples, with gauge sections of 2.2 mm wide by 2.2 mm thick and 4 mm long as presented in [28] were cut from the industrially manufactured cylinder heads made of A319 alloy through the Lost Foam Cast process (LFC), and all the samples were extracted from the fire deck area that is the most critical area in cylinder head. In order to assess the effect of various heat

treatments, listed in Table 2, on the microstructures of LFC A319 alloy, solution heat treatment at 495°C (i.e. below the incipient melting) at two different durations (i.e. 2 h 30 min and 50 h) were performed to dissolve the Al_2Cu phase at varying degrees. In order to estimate the sole effect of hard inclusions (i.e. eutectic Si, Al_2Cu phase) changes on the mechanical properties of the A319 alloy with different solution heat treatment conditions in a further study [28], over-aging treatments with different durations were performed to keep the same hardness of α-Al matrix after the two solution heat treatment conditions.

Table 2 : The heat treatment conditions used in this study

	Heat Treatment (HT1)	Heat Treatment (HT2)
Solution heat treatment	495°C for 2 h 30 min	495°C for 50 h
Quenching	Air cooling to room temperature	
Ageing	200°C for 150 h	200°C for 200 h

2.2 Microstructural characterization

In order to study the effect of various heat treatments on the evolution of the microstructural constituents amount, size and morphology in LFC A319 alloy, conventional 2D image analysis using OM and advanced 3D imaging using X-ray Laboratory Computed Tomography (Lab-CT) were used for the microstructural characterization. As the observed mechanisms were reproducible among these samples for same heat treatment condition, only one specimen for each condition (i.e. HT1 & HT2) is presented in this paper.

2.2.1 Characterization technologies

The measurement of pores, Al_2Cu and Iron-intermetallics characteristics were performed with Lab-CT at the ISIS 4D platform (Lille, France) using an Ultratom Lab-CT system from RX Solution fitted with a Nanofocus tube whose acceleration voltage was set at 80 kV. The specimen was placed on a rotating stage in the tomography chamber between the X-ray source and the detector. In order to characterize the microstructure evolution in 3D for LFC specimens during heat treatment, high resolution (voxel size of 2 µm) Lab-CT was performed on a same area for each specimen before and after heat treatment. The size of the scanned volume was 1200×1200×1300 voxels ($2.4×2.4×2.6mm^3$). For each scan, 2000 projections were taken while the sample was rotating over 360° along its vertical axis; with an acquisition time per image of 1100 ms, one scan lasted about 45 min.

As 3D characterization for the Si phase could not be achieved with Lab-CT because Al and Si have close atomic numbers hence similar X-ray attenuation [3], a 2D metallographic analysis at a pixel size of 0.07 µm was realized. Quantitative measurement of the eutectic Si particles characteristics was

performed with a Nikon YM-EPI light microscope equipped with a Sony color video camera. All the samples were polished using abrasive papers of grades up to 4000 grits in succession and then using polishing cloths and suspensions up to 1/4 μm. Finally, polishing was performed with a commercial 0.04 μm silica oxide colloidal suspension (OPS), until the sample surface becomes mirror like. The size and morphology of eutectic silicon phase was examined for each sample before and after heat treatment on polished samples; an average area of about 4.4 mm^2 was analyzed so as to represent the features of the whole sample.

2.2.2 Image processing

2D images obtained by optical microscope were analyzed by ImageJ/Fiji while 3D images were processed and analyzed using Avizo Fire software; the 3D images obtained in the as cast and heat-treated conditions were registered using Avizo before image analysis. Details about the quantitative analysis process are reported in [3]. Quantitative analysis could then be realized to label the objects: to attribute each individual object a given label or color, and to measure several characteristics of the labelled objects. According to B.M. Patterson et al. [29], image processing is critical to the quantification of features, in the present work, objects that are small as compared to the resolution of the images, with a volume less than 9 voxels were neglected and discarded from the analysis.

Feret diameter, sphericity and granulometry were the main parameters used to characterize the morphology of Fe-intermetallics, Al_2Cu, Si particles and pores. Feret diameter corresponds to the longest distance measured between two parallel tangents on each side of the 2D or 3D object of interest [30]. Feret diameter obtained from Avizo® Fire is estimated from the length of the longest side of the minimum bounding box, and it was used to assess the size of pores and hard inclusions, i.e. Fe-intermetallics, Al_2Cu, Si particles, compared with the commonly used 'Equivalent diameter', which is the diameter of a sphere that would have the same volume as the object, it could better reflect the 3D extent of objects. Sphericity, or circularity in 2D, is defined as the ratio between the particle area and the area of the circle with the same perimeter as the object in 2D [31] or as the ratio between the object volume and the volume of a sphere with the same surface as the object in 3D [3]. It tends towards 0 for infinitely elongated polygon and it equals 1 for a perfect circle, it is used to describe the characteristics of eutectic silicon in the literature [32,33]. Granulometry estimates 3D objects sizes using morphological opening operations: openings are performed step by step with an increasing structuring element size until all objects in the volume have disappeared in the input binary image. The number of non-zero pixels still present in the image is collected after each step [34]. Thus, granulometry reflects the local thickness distribution of a given phase in 3D. Besides, the local curvature of the 3D surface of Al_2Cu phase, which provides an indication of local variations in surface energy [35], was also studied. The mean curvature H is defined as: $H = 0.5 \times (1/R1 + 1/R2)$, where R1 and R2 are the two principal radii of curvature of the surface.

2.3 Hardness test

Hardness measurements were performed on the polished samples before and after both heat treatment conditions. Vickers hardness measurements were performed on the base alloys and α-Al matrix by using a load of 20 kg and 0.1kg respectively, dwell time is 15s. Each measurement represents the average of at least ten indentation readings taken from different areas of the specimen.

3 Results and discussion

3.1 Mechanical properties measurement

Typical microstructures of specimen HT1 are shown in Figure 1, it consists of α-Al, eutectic Si, Al_2Cu phase and iron-intermetallics. Due to the coarse microstructures induced by the low cooling rate of LFC, as seen in Figure 1(a), the Vickers hardness indent at very low load (0.1kg) is inside α-Al matrix hence it is suited for the determination of hardness of the α-Al matrix. The larger indent (20kg) in Figure 1(b) shows that it encompasses enough microstructural features to be representative of the overall alloy.

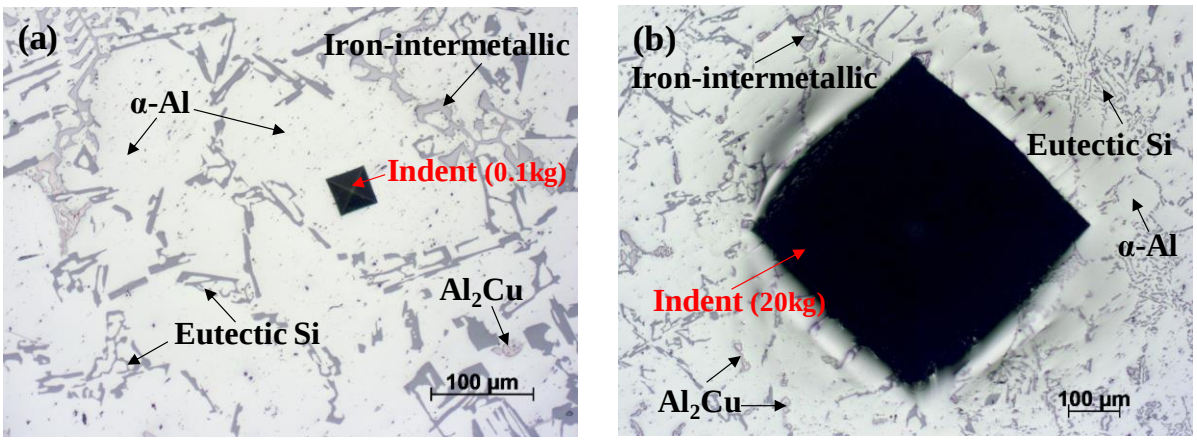

Figure 1: Optical micrograph showing the microstructure of specimen HT1: (a) a low load indent inside the α-Al matrix, (b) the large indent in the surface of base alloy.

Figure 2 shows the variation in hardness for the A319 base alloy and α-Al matrix at different heat treatment conditions. It can be seen that the α-Al matrix is softer than base alloy, and the average hardness level of base alloy decreased with increasing solution and aging time. This change was directly linked to dissolution of Al_2Cu phase because the hardness of Al matrix (2.1 GPa) [3] obtained from nanoindentation measurements is smaller than that of Al_2Cu phase (5.7 GPa) [36]. Thus, the reduction of the Al_2Cu volume fraction after solution heat treatment results in decreased hardness for the base alloy.

Despite a limited increase of hardness of α-Al matrix from 63±4 HV (standard deviation) to 66±3 HV (standard deviation) after HT1 treatment, the hardness of α-Al matrix after solution heat treatment and

aging is nearly the same as in the as-cast alloy, the difference is within the standard deviation as shown in Figure 2. Thus, the obtained samples can be used for the further investigation that estimates the effect of eutectic Si and Al_2Cu phase changes on the mechanical properties of the A319 alloy, and the results were presented [28].

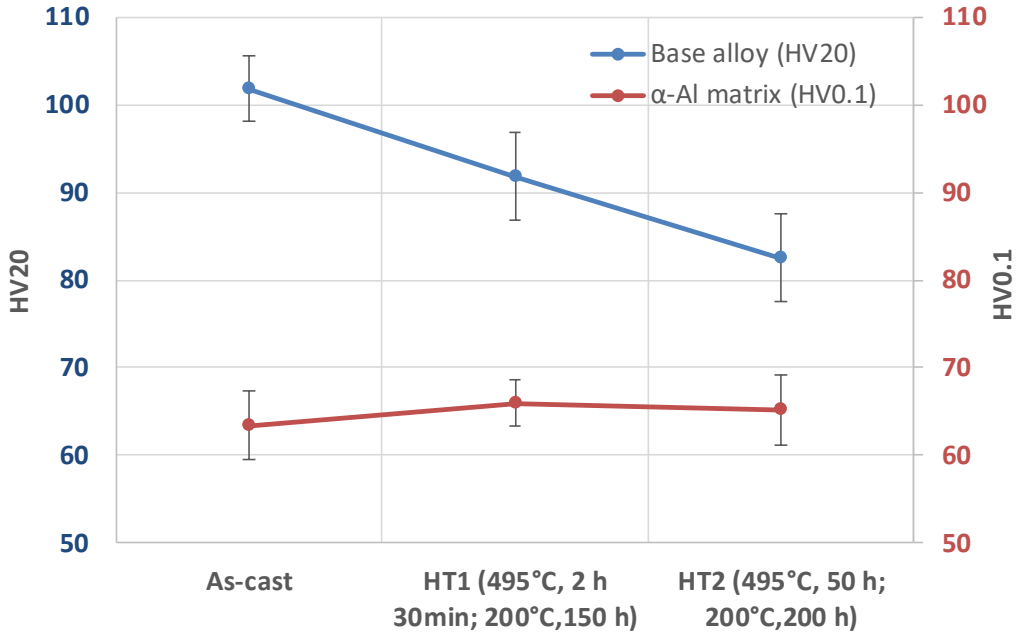

Figure 2 : Hardness as a function of various heat treatment conditions for base alloy and α-Al matrix

3.2 Pores

In order to avoid incipient melting of the copper-rich phase that would introduce micro pores, the temperature of conventional solution treatment for Al-Si-Cu alloys is restricted to 495°C [11]. In the present work, the solution temperature of all the specimens was thus 495°C, and the 3D characterization of pores was compared for two specimens (named HT1 and HT2 for the two heat treatment conditions in Table 2) before and after the heat treatment.

The volume fraction of porosity in specimens HT1 and HT2 range from 1.06% to 1.35%, which is close to that measured in the large volume of studied material without any heat treatment in reference [37]. Besides, the largest pores in specimens HT1 and HT2 have a Feret diameter from 2.1 mm to 2.3 mm, which is also the typical size for this material [3]. Thus, it indicates that the volume studied is representative.

Figure 3 shows the 3D rendering of the pores at a voxel size of 2 µm in specimen HT2 in as cast (Figure 3(a)) and heat-treated conditions (Figure 3(b)). The pores are visible in the specimens with different

condition and different colors indicate unconnected particles within the studied volume. As shown in Figure 3(c), the newly formed pores after the heat treatment were revealed by subtracting the image of the as cast specimen (Figure 3(a)) to the image of the heat-treated specimen (Figure 3(b)), more small formed pores were observed in specimen HT2 after heat treatment, especially on the edges of the sample. Figure 3(d) and (e) show the reconstructed 2D tomographic slices of the same region of the specimen HT2 at as cast condition and after 50 h of solution treatment at 495°C, respectively.

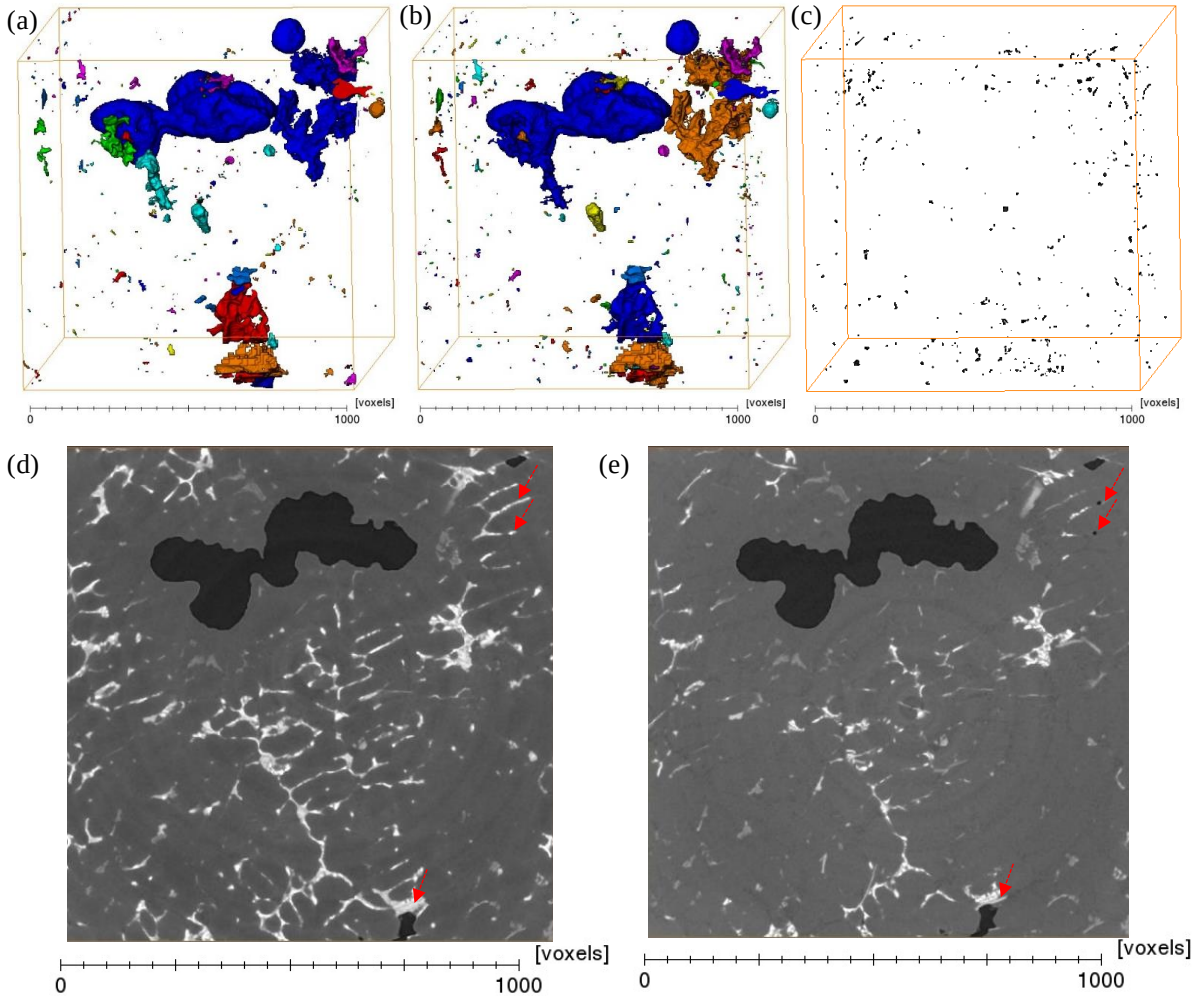

Figure 3: 3D rendering of pores in the ROI for specimen HT2, (a) as cast and (b) after heat treatment at 495°C for 50 h, (c) 3D rendering of newly formed pores in the ROI for specimen HT2 after heat treatment at 495°C for 50 h, (Dimensions: 2.1× 2.1×2.4 mm^3); different colors indicate unconnected particles within the studied volume. Tomographic images showing the formation of micro pores after the heat treatment by local melting of Al_2Cu of specimen HT2: (d) as cast, (e) 495°C, 50 h.

Samuel et al. [8] reported that the fine Al5Mg8Si6Cu2 phase start to melt at 505 °C in an A319 alloy during the heat treatment. Meanwhile, [38] found that incipient melting pores even occurred during solution treatment at temperature lower than common melting points of intermetallic phases. Given the

long duration of the heat treatments, i.e. 50h for present work, incipient local melting of fine Al5Mg8Si6Cu2 phase can be considered one of the reasons for the formation of small pores after heat treatment, as the red arrows indicated in Figure 3(d) and (e). Toda et al. [14] reported that the occurrence of incipient local melting of Al_2Cu in Al-Si-Cu alloy during solution heat treatment leads to the growth of micro pores adjacent to the melt regions. Besides, Li et al. [20] reported that the dissolution of small Al_2Cu phases takes place by radial diffusion of Cu atom into the surrounding matrix, according to the atomic diffusion theory [38], temperature, diffusing time, as well as diffusion distance and concentration gradient play a significant role in affecting incipient melting process. Thus, the diffusion of Cu atom could also possibly lead to the formation of small pores after long duration of heat treatment [39]. In addition, S. Lippmann et al. [40] reported that the local curvature of second phases can also affect the melting point depression, this will be discussed later in more details (section 3.4).

The pores characteristics of specimen HT1 and HT2 before and after heat treatment are summarized in Table 3, while the distributions of pores are shown in Figure 4. As seen from Figure 4, the first peak in the Feret diameter distribution corresponds to small pores with a size about 20~30μm in both specimens, and the heat treatment introduces more fine pores in the range of 6–40 μm and 6–60 μm for specimen HT1 and HT2, respectively, especially in specimen HT2. The total number of pores increased from 623 to 806 after 50 h of solution treatment at 495°C (Table 3). The slight variation of volume fraction of porosity between the as cast and heat-treated condition is within the measurement error, these small pores formed after heat treatment do not have a sufficient contribution to increase the volume fraction. However, the nucleation of small pores after heat treatment results in a decrease of the average size of the pores in both specimens.

Table 3 : Porosity characteristics in both specimens before and after heat treatment.

Specimen	**Heat treatment condition**	**Volume fraction %**		**Number**		**Feret diameter (μm)**				**Analysed volume (mm^3)**
						Av.		**Max.**		
		As-cast	Heat-treated	As-cast	Heat-treated	As-cast	Heat-treated	As-cast	Heat-treated	
HT1	495°C, 2 h 30 min + 200°C,150 h	1.07	1.06	482	623	74.4	62.4	2177	2153	10.58
HT2	495°C, 50 h + 200°C, 200h	1.35	1.31	533	806	68.6	58.3	2304	2306	

The results evidenced that incipient melting of Al_2Cu phases has occurred during solution treatment at 495°C, especially for long time heat treatment, i.e. 50 h , which results in the small pores formation, this is inconsistent with the findings of [8].

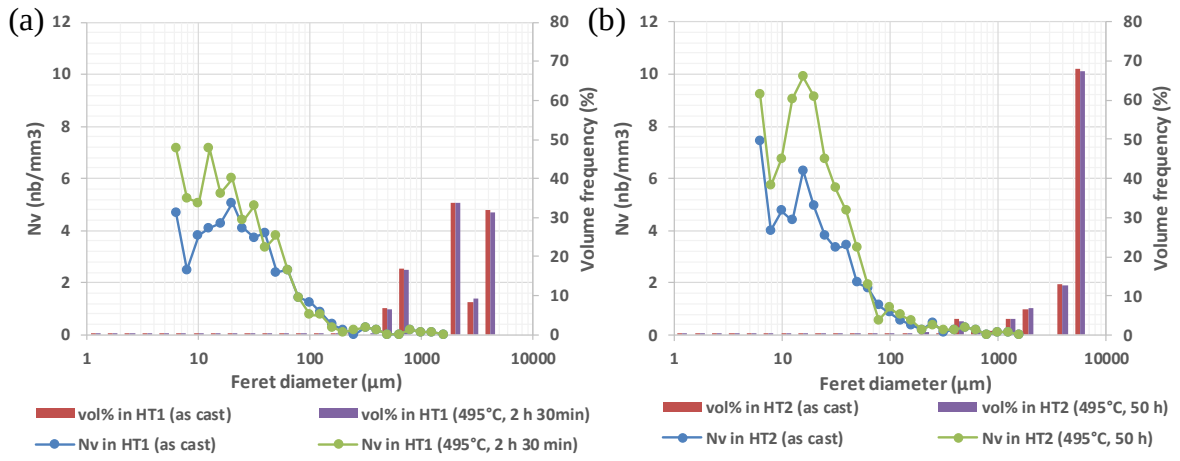

Figure 4 : Size distribution of pores in number (Nv) and in volume (%) for specimen (a) HT1 and (b) HT2 before and after heat treatment.

3.3 Eutectic Si characterization

The morphology evolution of eutectic Si as function of heat treatment time is demonstrated in Figure 5. Eutectic Si without heat treatment (as-cast) occurred in platelets form (see the white arrows in Figure 5(a)). With a short solution time (2 h 30 min), some platelets Si particles were fragmentized into smaller platelets with rounded edges (see the yellow arrows in Figure 5(b)). With a longer solution treatment at 495°C for 50 h , the fragmented particles were partly spheroidized while some smaller Si particles were spheroidized to fully circular shape (see the red arrows in Figure 5(c)).

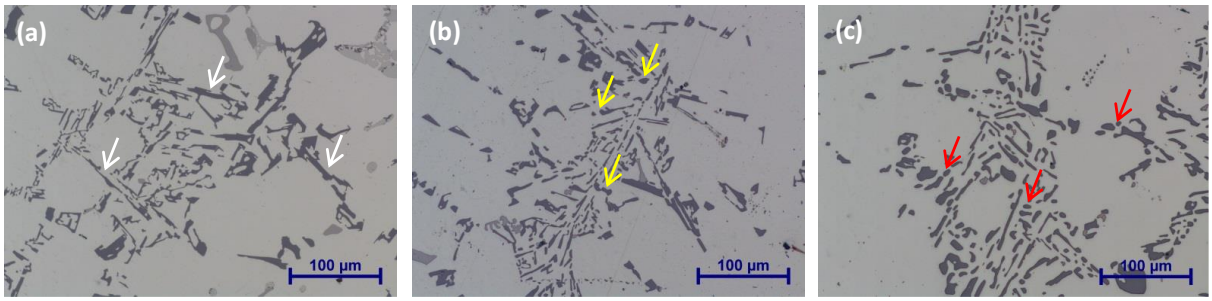

Figure 5: Microstructure of Al-Si-Cu alloy showing the morphology of Al-Si eutectic; (a) as-cast condition, (b) after solution treatment at 495°C for 2 h 30 min (HT1) and (c) after solution treatment at 495°C for 50 h (HT2)

Quantitative metallographic characterization of eutectic Si particles was performed on the samples with different heat treatment conditions using image analysis in terms of average Si particles area (µm²),

average Si particles length (µm) and circularity. Figure 6(a) shows that the surface fraction of large particles (Feret diameter > 50µm) decreased with increasing solution time.

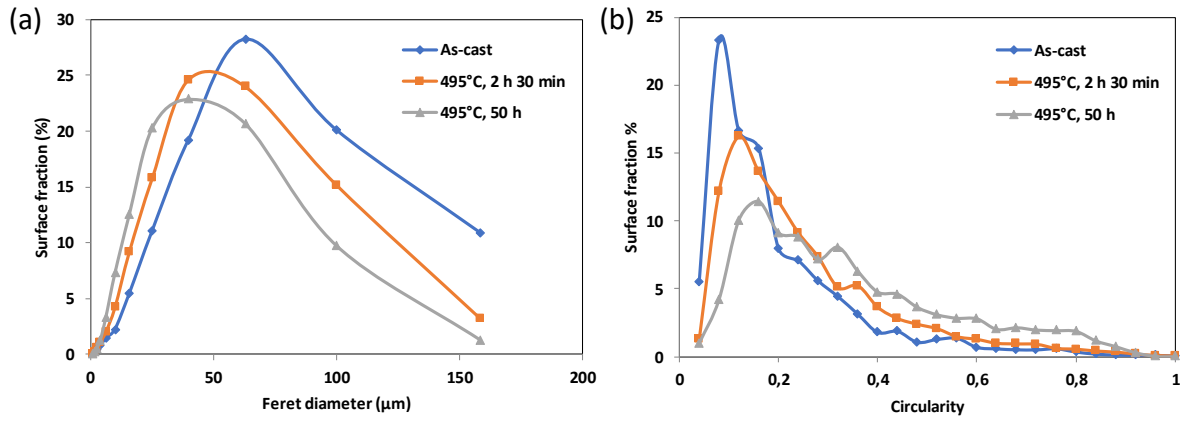

Figure 6: Distributions of (a) Feret diameter and (b) circularity of eutectic Si particles in studied Al-Si-Cu alloy in as-cast condition and for HT1 and HT2 solution treatment

As Table 4 shows, in the as-cast condition, the Si platelets have an average length of 10.52 µm. After the heat treatment for 2 h 30 min at 495°C, the average Si particles area and length decreased (taking into account the standard deviation), whereas the Si particles density increased by about 80%, *i.e.* from 1416 to 2560 particles/mm². These results show that the Si platelets underwent partial fragmentation. When the solution time increased to 50 h, the average Si particles area, length and the particles density decreased slightly. Besides, the decrease in the Si particles density from 2560 particles per mm² to 2050 with heat treatment increase from 2 h 30 min to 50 h (Table 4) may be attributed to the coarsening of Si particles.

Table 4 : Silicon particles characteristics evolution with solution treatment durations

Heat treatment condition	Particle area (µm²)		Particle length (µm)		Density (particles/mm²)
	Average	Standard deviation	Average	Standard deviation	
As-cast	46.0	137.5	10.5	17.0	1416
HT1	35.0	95.7	10.0	13.9	2560
HT2	34.8	82.2	9.3	11.8	2050

In addition, the heat treatment can affect the morphology of the eutectic Si particles. The distribution of circularity of eutectic Si particles is plotted as a function of solution time in Figure 6(b). More eutectic Si particles with circularity between 0.05 and 0.2 were present in as-cast sample as compared to samples

heat treated at 495°C. Increasing the solution time from 2 h 30 min to 50 h, increases the amount of particles with circularity above 0.3. This means that the amount of eutectic Si with plate-like morphology decreased with an increase of solution treatment time: the longer the solution treatment, the more eutectic Si shows a globular morphology. Therefore, the experimental evidence indicates that increasing the solution treatment time causes the plate-like eutectic silicon phase to become fragmented and spheroidal in shape.

The eutectic silicon morphology, viz., particles size and shape, plays an important role in determining the mechanical properties in A1-Si alloy castings [41]. As a thermal modification, heat treatment is being used in conjunction to produce the desired properties of a casting Al-Si alloy [42]. As shown in Figure 5(a), the silicon particles were coarse, acicular needles in the as-cast LFC A319 alloys, and after a solution heat treatment as shown in Figure 5(b) and Figure 5(c), the silicon particles were modified. This morphological evolution may be interpreted as follows: the fragmentation and spheroidization of the eutectic Si particles in the studied LFC A319 alloy occur when the alloy is subjected to solution heat treatment at 495°C and increase as the solution treatment time increases from 2 h 30 min to 50 h, as reflected in the continual increase in the Si particles circularity. During solution heat treatment, silicon particles are initially broken down into smaller fragments that are then gradually spheroidized.

The effect of heat treatment on the morphology of eutectic silicon has been widely reported [16,43]. M.A. Moustafa et al. [44] reported that silicon particles usually undergo fragmentation, spheroidization and coarsening during solution treatment. However, the present work does not show strong evidence for the coarsening of Si particles except the decrease of Si particles density from 2 h 30 min to 50 h solution heat treatment. This might be because the fragmentation is the main process at the early stage of the solution heat treatment for this alloy. With the progress of solution treatment time, fragmentation and coarsening occur together as a whole. The fragmentation counterbalances the effect of coarsening based on the quantitative size analysis. In addition, the coarsening of Si particles is more evident in the case of a long or a high temperature heat treatment, *e.g.* [45] reported that the effect of Si coarsening is more pronounced after 80h solution heat treatment at 540°C in an non-modified A356 alloy.

3.4 Al_2Cu phase

As reported in [20], copper forms an intermetallic phase with aluminum that precipitates during solidification either as block-like Al_2Cu or in eutectic form as ($Al+Al_2Cu$). These copper containing phases are easily distinguishable under X-ray tomography (voxel size = 2µm).

In order to study the effect of solution heat treatment on the dissolution of the Al_2Cu phase, the characteristics of the Al_2Cu phase were quantitatively examined through Lab-CT in the as-cast state and after two solution treatment durations. The 3D analysis provides detailed information regarding the spatial distribution of the Al_2Cu phase. 3D renderings of Al_2Cu phase in specimens HT1 and HT2 before

and after the heat treatment are shown in Figure 7 and Figure 8 respectively. The dissolution increased with increasing solution time (2 h 30 min to 50 h) at 495°C.

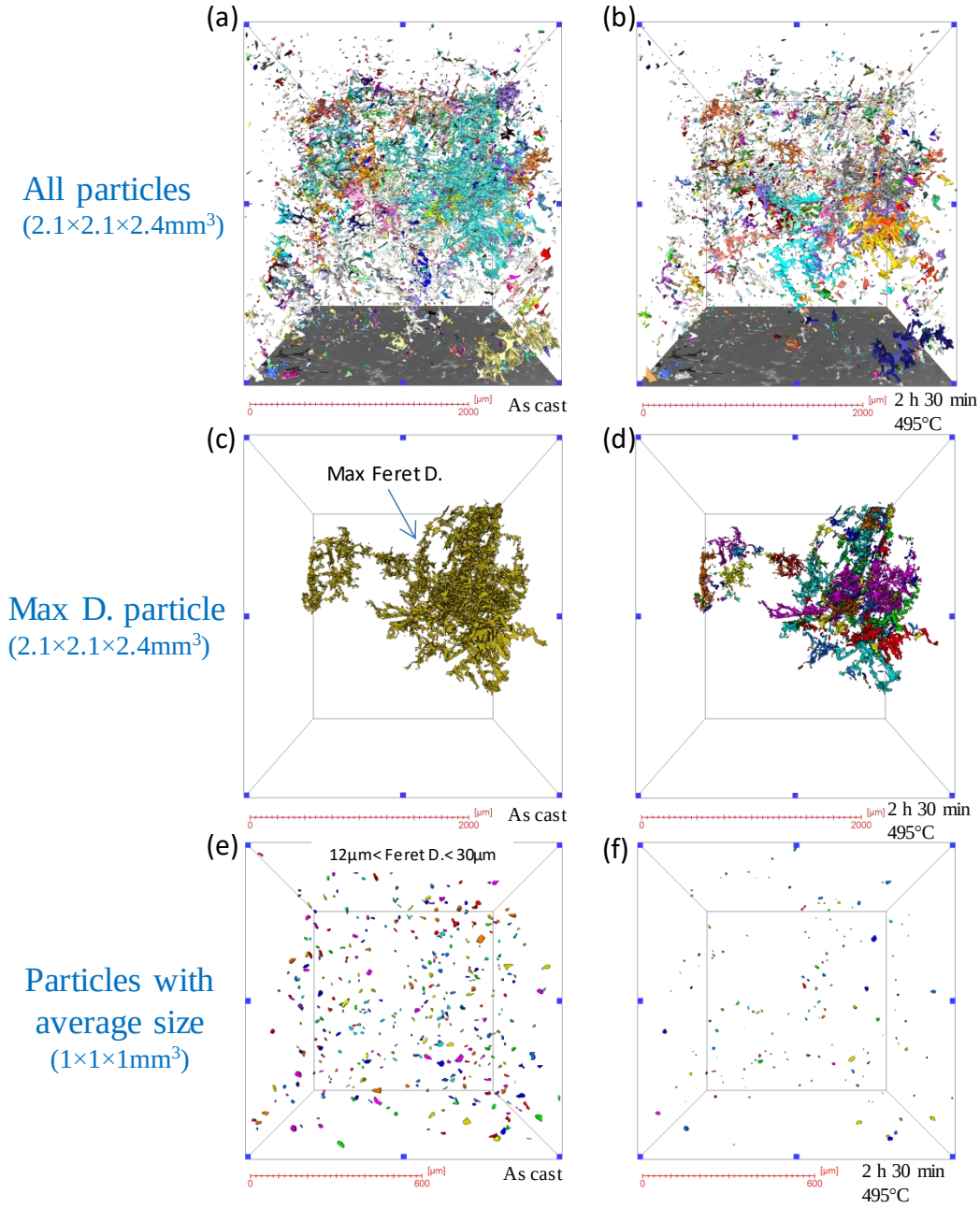

Figure 7: 3D rendering of the Al_2Cu phase, from top to bottom: all the particles and the largest particle in the same 2.1×2.1×2.4 mm^3 region, particles having a Feret diameter between 12 to 30µm in a sub-volume (1×1×1 mm^3) at: (a, c and e) as-cast condition and (b, d and f) after 2 h 30 min at 495 °C for specimen HT1

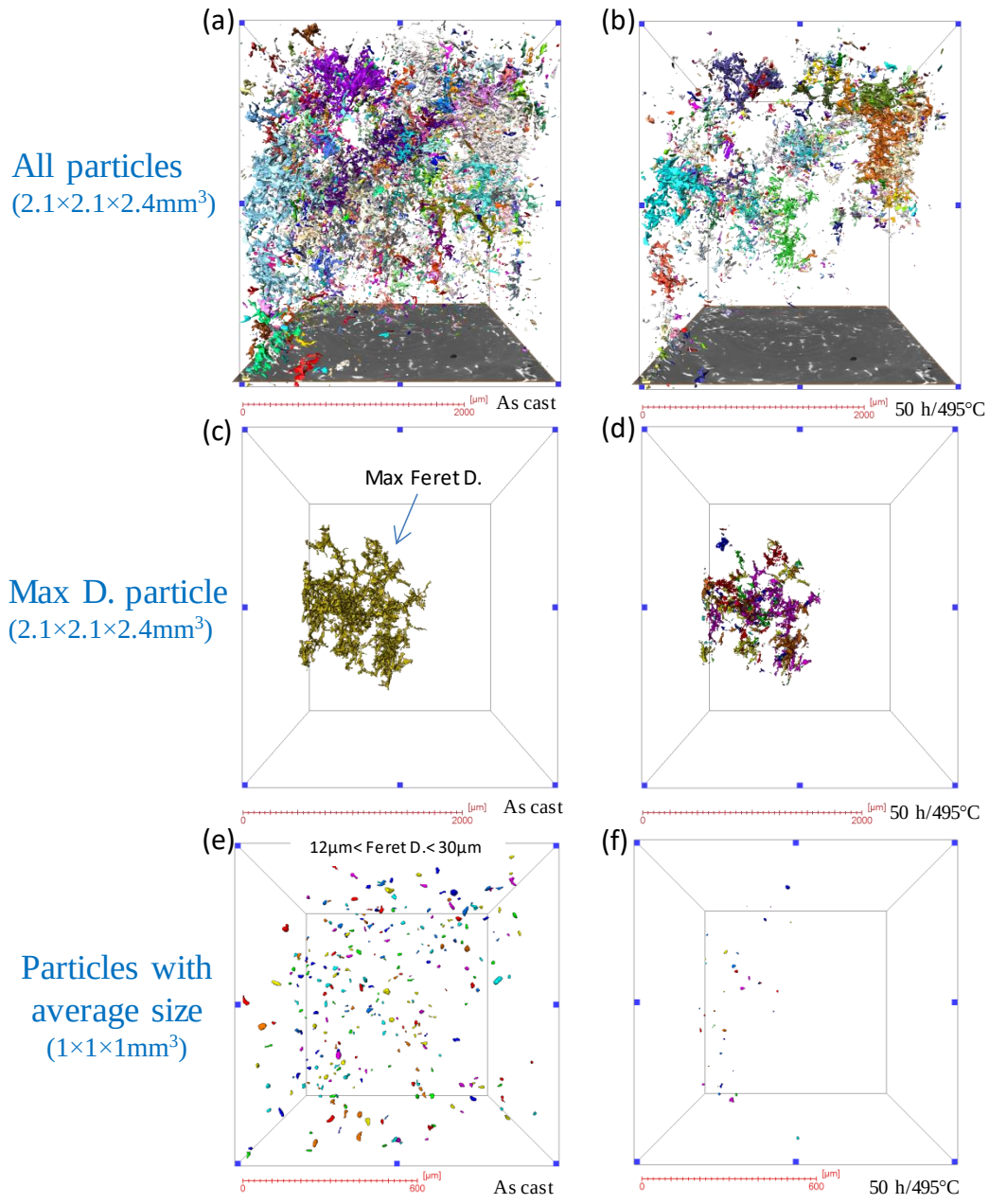

Figure 8: 3D rendering of the Al_2Cu phase, from top to bottom: all the particles and the largest particle in the same 2.1×2.1×2.4 mm^3 region, particles having a Feret diameter between 12 to 30µm in a sub-volume (1×1×1 mm^3) at: (a, c and e) as-cast condition and (b, d and f) after 50 h at 495 °C for specimen HT2

Firstly, the heat treatment reduces the number of objects, i.e. unconnected Al_2Cu particles. The number of Al_2Cu particles of specimen HT1 decreased from 13999 to 7930 in a volume of 10.58 mm^3 (ROI for tomography analysis) after the 2 h 30 min solution treatment.

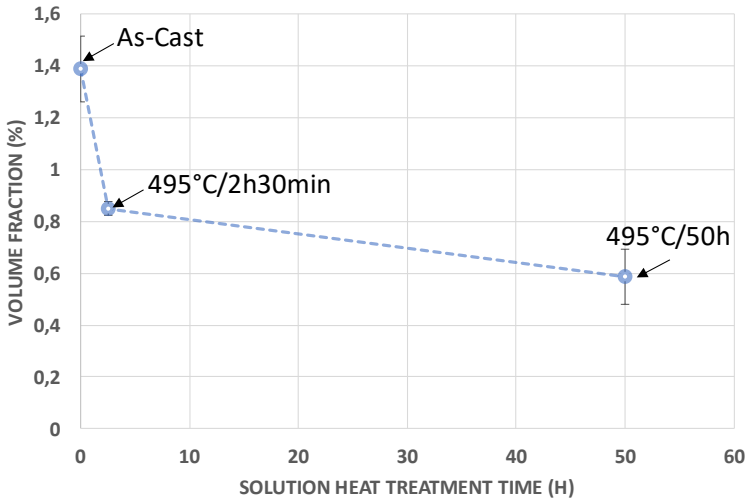

Figure 9: Al_2Cu phase dissolution in the studied specimens during solution heat treatment at 495°C as a function of solution treatment time

The volume fraction of undissolved Al_2Cu phase was measured as a function of solution heat treatment time and plotted in Figure 9, it should be noted that this result with the standard deviation is based on the analysis of two specimens for each heat treatment condition. After a solution treatment of 2 h 30 min at 495°C, the volume fraction of Al_2Cu phase decreased significantly from about 1.4 % to 0.86%, i.e., about 33% of the total Al_2Cu phase has been dissolved in the matrix. With an increase in the solution treatment time to 50 h, the Al_2Cu phase dissolution becomes slow, reaching a volume fraction of 0.66%, i.e. about 58% of Al_2Cu phase was dissolved. As shown in Figure 9, the dissolution process speed is higher during the first 2 h 30 min solution treatment, this is because particles that are smaller than the average particle size take short to dissolve [46], it will be discussed in details in the following part. Dissolution kinetics of Al2Cu phases in Al-Si-Cu alloy is widely studied in literature [46–49]. It depends on several factors, such as temperature, diffusion distance (i.e. secondary dendrite arm spacing), particle morphology, and so on. Many models have been developed to help gain the knowledge of dissolution kinetics in order to better design the heat treatment process. Aron [47] firstly proposed a model for dissolution of second phase particles. Afterward, Whelan [48] expanded the model to take into account the steady state and transient parts of the dissolution kinetics. Brown [49] considered the influence of spherical, cylindrical and planar shapes on the dissolution kinetics. More recently, Sadeghi et al. [46] proposed a model to predict the dissolution of secondary phases including Al_2Cu and Q phases in B319 alloy. According to his study, dissolution times are increased by increasing SDAS or decreasing solution temperature, both the modelling and experimental results show that at 500 °C dissolution is more or less complete after 4 h for B319 alloy with SDAS of 39 µm. However, in the present work, there is only the as cast microstructure (t=0s) and the microstructure after solution heat treatment at 495°C either for t=2h30min or t=50h. Two points are not enough to draw a kinetic dissolution law and check if the radius

decrease that is predicted with Aaron or Whelan laws can match the local evolution observed in Figure 9.

In addition, the largest Al_2Cu particles in each sample at different conditions are shown in Figure 7 and Figure 8(c) and (d) separately. The loss of interconnectivity is revealed by the increase in the number of particles (different colours represent unconnected particles). As shown in Figure 10(a) and (c), the size of the largest Al_2Cu particle decreased after the heat treatment. Besides, Figure 10(a) and (c) show that the number of particles with small and average size significantly decreased after the heat treatment. This result can be illustrated through the 3D rendering of Al_2Cu particles having a size that ranges from 12 µm to 30 µm in the sub-volume shown in Figure 7-8(e) and (f). After 50 h at 495°C, most of the particles with average size have disappeared.

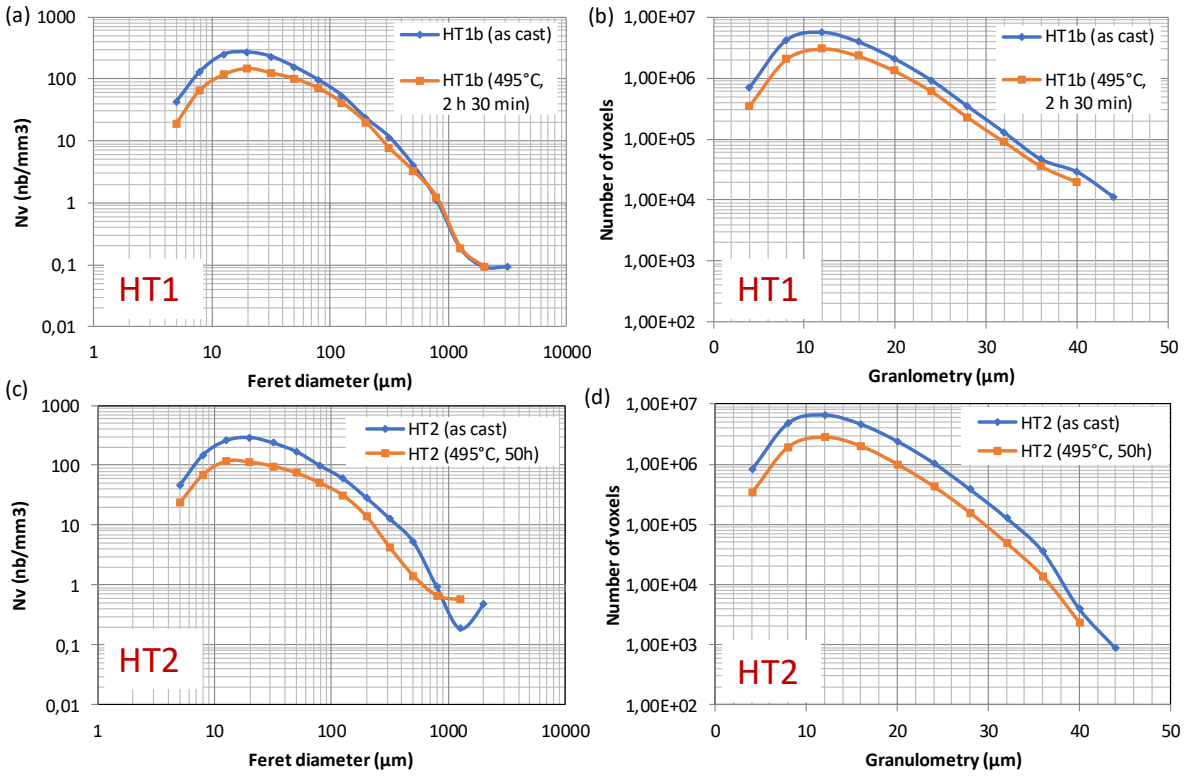

Figure 10: Distributions of Al_2Cu phase as functions of Feret diameter and granulometry in as-cast and solution heat treated conditions for specimen HT1 (solution heat treatment of 2 h 30 min) and HT2 (solution heat treatment of 50 h)

Figure 10(c) shows more large size (i.e. around 1260µm) Al_2Cu particles in specimen HT2 after 50 h heat treatment than in as cast condition. This could be attributed to the disintegration of the structure at thinner sections of the largest Al_2Cu particle after heat treatment, which results in several new large size particles. The granulometry distributions of Al_2Cu phase in Figure 10(b) and (d) show that the thickness of all Al_2Cu particles decreases after the heat treatment in both conditions, especially for the particles

with average thickness (~12 µm). The maximum thickness of Al_2Cu phase was found to decrease from 44 µm to 40 µm in specimen HT1 and HT2 after heat treatment, which indicates that the large Al_2Cu particles are dissolved into smaller ones through heat treatment.

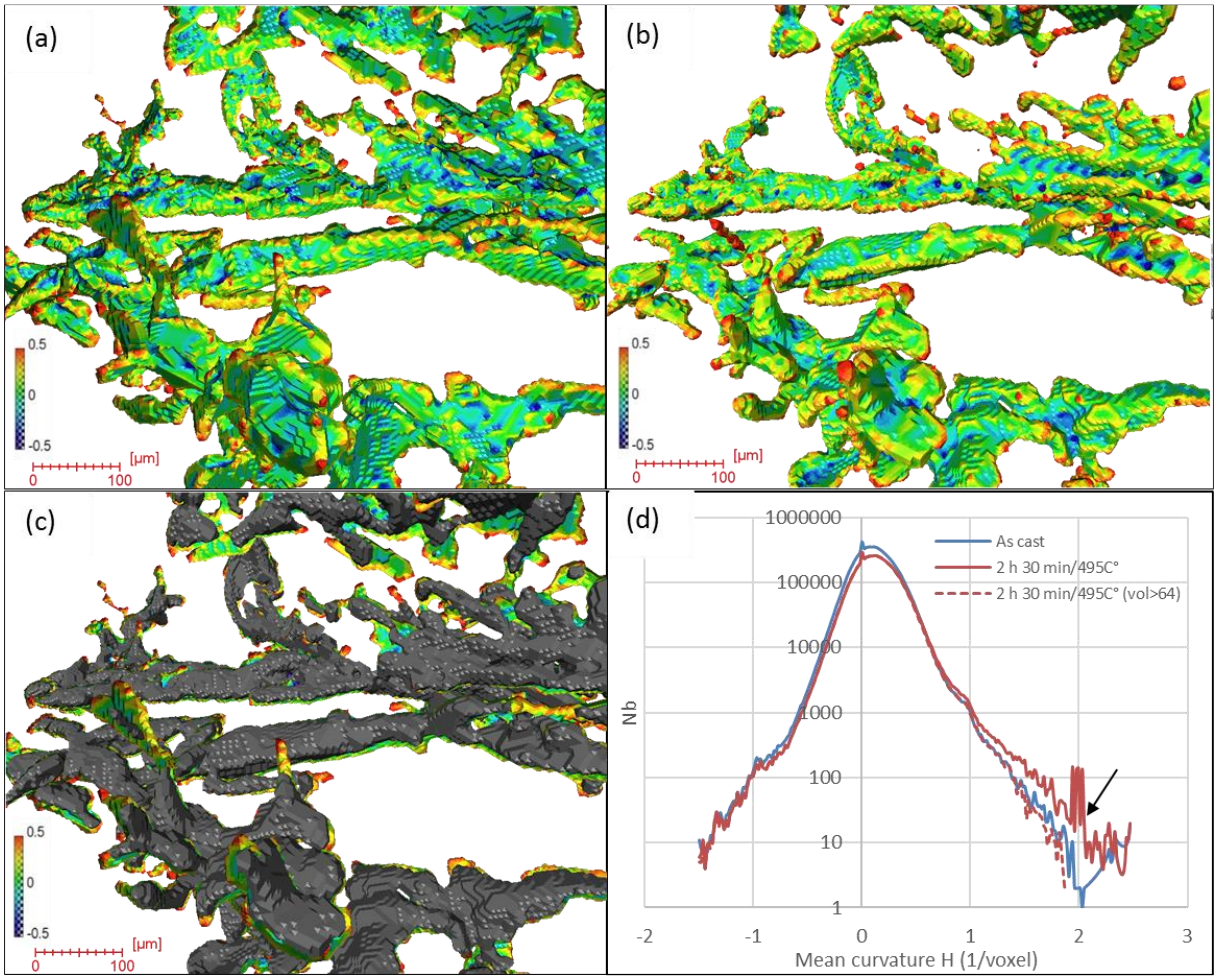

Figure 11 : 3D rendering of the Al_2Cu particle, (a) as-cast condition and (b) after 2 h 30 min at 495 °C, the colour represents the mean curvature values at the interface location, (c) 3D rendering of the Al_2Cu particle with black colour after 2 h 30 min at 495 °C is superimposed on the 3D rendering of the Al_2Cu particle in as-cast condition, (d) mean curvature distribution in as-cast and solution heat treated conditions for the largest Al_2Cu particle in specimen HT1.

In order to better understand the local evolution of Al_2Cu phases during the heat treatment process, typical 3D volume rendering of the largest Al_2Cu particle (in the as-cast condition) in specimen HT1 and HT2 with their mean curvatures distributions (H) before and after heat treatments are shown in Figure 11-12 (a) and (b). The green colour corresponds to a flat surface (H=0), whereas the red colour indicates a curved convex surface (H>0), the cyan color means local pit or groove (H<0) [35]. The Al_2Cu phases form a spatially interconnected complex 3D network, whose dissolution can be observed during the heat treatment process, especially for specimen HT2 (Figure 12(a) and (b)). The distributions

of the mean curvatures for Al_2Cu phases are shown in Figure 11-12 (d). 3D rendering of Al_2Cu phases after 2 h 30 min at 495 °C is superimposed with black colour on the 3D rendering of Al_2Cu phases in as-cast condition (see Figure 11(c)). The remaining colour-coded voxels show the dissolution area of Al_2Cu phases and highlight that the regions with high curvatures, in red, have disappeared after heat treatment. However, as indicated by the arrow in Figure 11(d), surfaces with high positive curvatures (H>1) tend to increase in number after 2 h 30 min at 495 °C in specimen HT1, The quantitative analyses show that the number fraction of triangles having high positive curvatures (H>1) increased from 0.1 % for as cast specimen to 1.5 % for the specimen after a 2 h 30 min solution heat treatment at 495 °C. The reason can be that the newly formed small particles due to the fragment of the largest Al_2Cu particle create new high curvature regions compared to the initial Al_2Cu particle. For specimen HT2, the distribution of mean curvatures shows that mean curvatures less than 1 were decreased in number after a 50 h solution heat treatment at 495 °C because of the large amount of Al_2Cu dissolved in the matrix (as can be seen from Figure 12 (c)). While, the high positive curvatures (H>1) increased from 0.35 % for as cast specimen to 0.78 % for the specimen HT2 after 50 h at 495 °C due to the newly formed small Al_2Cu particles. This also can be proved by the fact that removing the particles less than 64 voxels in volume (objects less than 4*4*4 voxels) show a large effect on the highest mean curvature region of the histogram (dotted red line in Figure 11-12 (d)).

Heat treatment affects the microstructure by causing the fragmentation and dissolution of the Al_2Cu phase during solution treatment [20]. The average volume fraction of Al_2Cu in the studied alloys decreased from 1.4% in the as-cast condition to 0.66% after the 50 h solution treatment at 495°C. Meanwhile, we observe from Figure 7~Figure 12 that the Al_2Cu phase undergoes morphological and size changes during solution heat treatment.

During the first 2 h 30 min of solution heat treatment at 495°C, the Al_2Cu phase undergoes the fragmentation of the larger Al_2Cu particles by pinching off the thinner arms (see Figure 7(c) and (d)) and by the dissolution of average size Al_2Cu particles (see Figure 7(e) and (f))) with radial diffusion of Cu atoms into the surrounding aluminum matrix. The evolution of local curvatures of the Al_2Cu phases during the heat treatment allows a better understanding of the dissolution mechanisms. Owing to Gibbs-Thomson effects, the high positive curvature at the tip of these particles have higher dissolution pressure [50], therefore, these regions favour dissolution of the particle in the early stage of heat treatment (see Figure 11(c) and (d)).

In the following 50 h of solution heat treatment, the volume fraction of Al_2Cu phase decreases further. The main process of fragmentation and dissolution of the Al_2Cu particles involves the disintegration of the structure at the thinnest sections of the Al_2Cu particles and the dissolution of the smallest Al_2Cu particles in the aluminum matrix in the same time period. However, comparison of Figure 8(d) and (f) shows that the fragmentation of the large Al_2Cu particles takes more time than the dissolution of Al_2Cu

particles with smaller radii. After 2 h 30 min of solution heat treatment, almost all the smaller particles have indeed already disappeared as can be observed from the comparison of the size distributions of Al_2Cu phase in samples HT1 and sample HT2 in Figure 10. This result can be explained by the classical Lifshitz–Slyozov–Wagner (LSW) theory for Ostwald ripening [51]. The LSW theory describes that solubility in the small particles with a large surface area-to-volume ratio is higher than that for larger particles [52], thus, the dissolution of small particles is easier during the heat treatment. These observations are in good agreement with the conclusions drawn by [53] and [54]. [53] reported that the blocky Al_2Cu phase particles are difficult to dissolve during solid solution heat treatment, unlike the fine Al_2Cu phase particles that can dissolve within 2 h of solid solution heat treatment. [54] found that the blocky Cu phase in B319 alloys may be partially dissolved with increasing solution heat treatment time at the recommended solution temperature of 495°C.

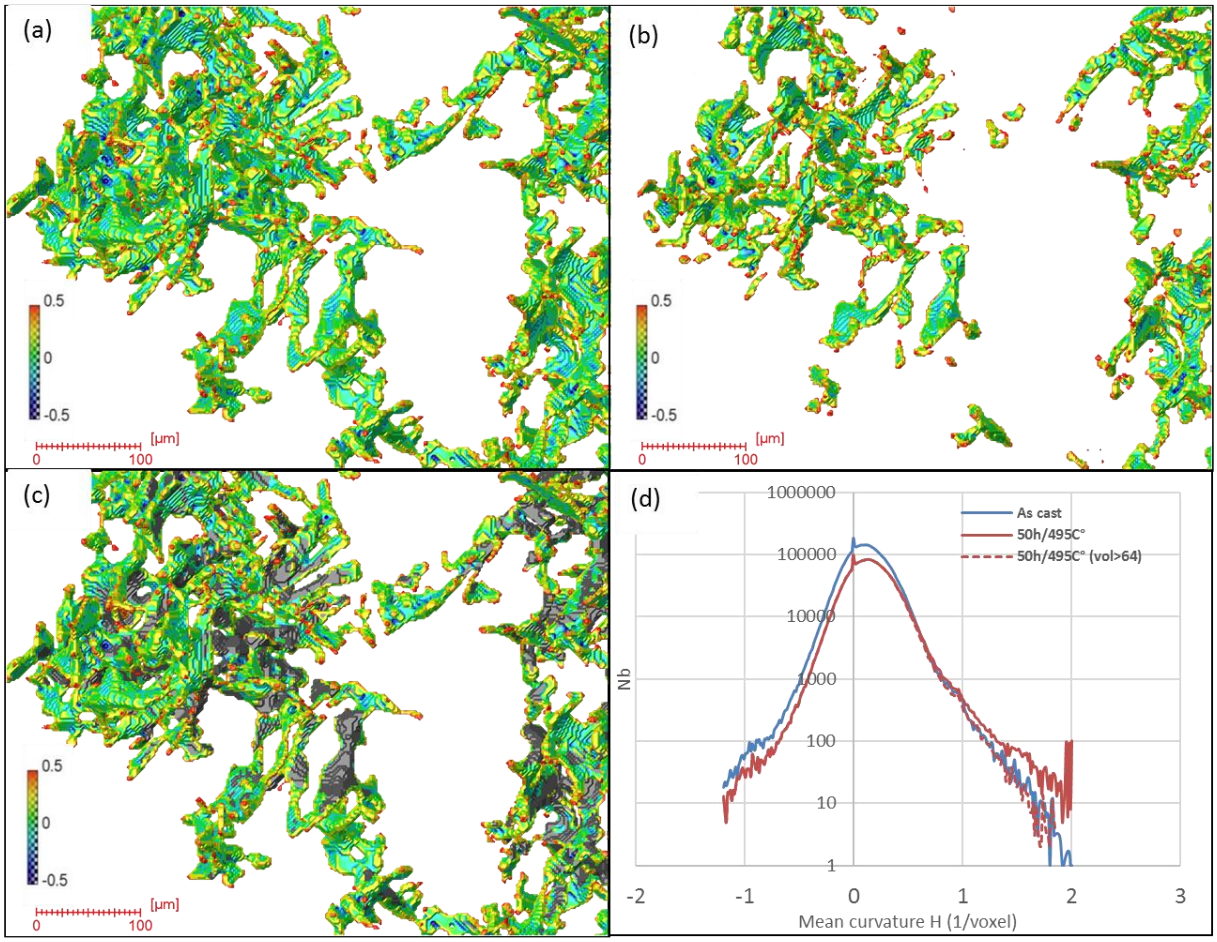

Figure 12 : 3D rendering of the Al_2Cu particle, (a) as-cast condition and (b) after 50 h at 495 °C, the colour represents the mean curvature values at the interface location, (c) 3D rendering of Al_2Cu particle with black colour after 50 h at 495 °C is superimposed on the 3D rendering of Al_2Cu particle in as-cast condition, (d) mean curvature distribution in as-cast and solution heat treated conditions for the largest Al_2Cu particle in specimen HT2.

3.5 Iron-intermetallics

In this work, iron-intermetallic characteristics were also studied in the as-cast condition and after both heat treatment durations, the results of quantitative 3D analysis by Lab-CT are summarized in Table 5. The heat treatment of 2 h 30 min at 495°C has no obvious effect on the volume fraction of iron-intermetallic in the specimen HT1. However, for specimen HT2, a slight decrease in volume fraction of iron-intermetallic phase was observed after the heat treatment at 495°C for 50 h. These results suggest that long heat treatment time might affect the fragmentation and dissolution of iron-intermetallics.

Table 5 : Volume fraction of Iron-intermetallic as a function of heat treatment time

Specimen	Heat treatment (H/T) condition	Volume fraction (%)			Max Feret diameter (µm)		Av. Feret diameter (µm)	
		Before H/T	After H/T	Diff.	Before H/T	After H/T	Before H/T	After H/T
HT1	495°C, 2 h 30 min + 200°C, 150 h	4.52	4.48	0.04	3636	3613	21 ± 40	25 ± 50
HT2	495°C, 50 h + 200°C, 200h	4.49	4.00	0.49	3753	3740	20 ± 39	24 ± 50

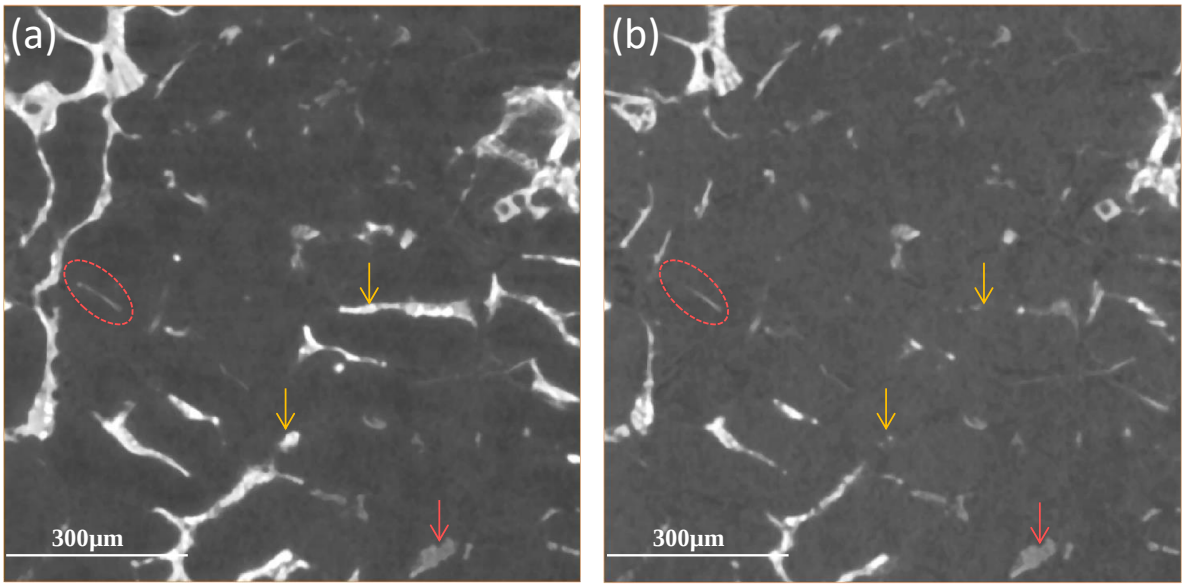

Figure 13: Tomographic images showing the effect of heat treatment at 495°C on the microstructure of specimen HT2: (a) 0 h, (b) 50 h

No noticeable changes were detected in specimens HT1 as regards the Fe-intermetallic phase before and after the 2 h 30 min heat treatment at 495°C. The slight decrease of volume fraction of Fe-intermetallics in specimen HT2 might be due to the dissolution of β-Al_5FeSi phase during long solution heat treatment.

Figure 13 displays reconstructed 2D tomographic slices of the same region of the sample HT2 at as cast condition and after solution treatment. The dissolution of Al_2Cu (yellow arrow) was observed clearly. In contrast to the α- phase (see red arrow) which remains unchanged during heat treatment, the needle-like β-phase (see red dotted circle) seems to undergo partial dissolution during solution treatment of 50 h at 495°C. These observations confirm the findings of [43] that the partial dissolution of the β-phase occurs after solution treatment for 24 h at 500°C while no noticeable changes occur for α-phase after solution treatment.

4 Conclusion and perspective

The effect of solution heat treatment on the microstructure of LFC A319 alloy was studied by optical microscopy and X-ray tomography. The temperature of solution heat treatment was 495°C and the solution time ranged from 0 to 50 h (0, 2 h 30 min and 50 h). The comparison of the microstructure in as-cast and different heat treatment conditions has led to the following conclusions:

1. The main processes that take place during solution treatment are: the dissolution of Cu in the Al matrix and the fragmentation and spheroidization of the eutectic Si.

2. Al_2Cu phase presents a highly interconnected 3D network in as-cast alloy, the solution heat treatment results in dissolution of the Al_2Cu phase that evolves in the following processes. In the early stage of heat treatment, the small Al_2Cu particles and the tip regions of the Al_2Cu particles with the high positive curvature were dissolved. The loss of interconnectivity by pinching off arms of the larger Al_2Cu particles generates small disconnected particles with high curvature. Further dissolving of the disconnected particles and the smallest Al_2Cu particles occurs by radial diffusion of Cu atoms into the surrounding Al matrix.

3. The morphology of the eutectic Si particles changes with solution treatment time; it undergoes the following transformations: fragmentation and spheroidization during the solution treatment.

4. A few needle-like β-Fe particles undergo partial dissolution after 50 h of solution treatment at 495°C. However, there were no noticeable changes for α-phase.

5. The incipient melting of Al_2Cu phase was assumed to occur after 50 h of solution treatment at 495°C, which leads to the formation of small pores, however, the volume fraction of porosity remains stable.

In the present work, two heat treatments were coupled with 2D/3D characterization of the microstructure to identify different hard inclusions characteristics while keeping the same hardness of matrix in LFC A319 alloy. This study is a preliminary work before studying the effect of hard inclusions changes, i.e. eutectic Si spheroidization, Al_2Cu phase dissolution, on the damage mechanisms of A319 alloy. The

results are presented in author's other paper [28]. Besides, the obtained results of the Al_2Cu phase dissolution mechanism could also help to optimize nominal solution treatment process to homogenize the alloys enough and ensure a satisfactory degree of precipitate dissolution.

5 Acknowledgements

The authors gratefully acknowledge the ANR (Agence Nationale de la Recherche) MatetPro project INDiANA (ANR-12RMNP-0011) for funding this study, and would like to thank ISIS4D (https://isis4d.univ-lille.fr/) X-Ray CT platform (Lille, France) for 3D microtomographic acquisition. The ISIS4D X-Ray CT platform has been funded by International Campus on Safety and Intermodality in Transportation (CISIT), the Nord-Pas-de-Calais Region, the European Community and the National Center for Scientific Research. The authors would like to thank Pierre Osmond from PSA Peugeot Citroën for providing the material and doing the heat treatment test of this study, and thank the China Scholarship Council (CSC) for funding the PhD thesis of Zaidao Li.

6 Data Availability Statement

All relevant data used to support the findings of this study are available from the corresponding author upon request.

7 References

[1] J.Y. Hwang, H.W. Doty, M.J. Kaufman, The effects of Mn additions on the microstructure and mechanical properties of Al–Si–Cu casting alloys, Mater. Sci. Eng. A. 488 (2008) 496–504. doi:10.1016/J.MSEA.2007.12.026.

[2] L. Wang, Influence of the casting microstructure on damage mechanisms in Al-Si alloys by using 2D and 3D in-situ analysis, Ecole Centrale de Lille, 2015.

[3] Z. Li, N. Limodin, A. Tandjaoui, P. Quaegebeur, P. Osmond, D. Balloy, Influence of Sr, Fe and Mn content and casting process on the microstructures and mechanical properties of AlSi7Cu3 alloy, Mater. Sci. Eng. A. 689 (2017) 286–297.

[4] M. Okayasu, Y. Ohkura, S. Takeuchi, S. Takasu, H. Ohfuji, T. Shiraishi, A study of the mechanical properties of an Al–Si–Cu alloy (ADC12) produced by various casting processes, Mater. Sci. Eng. A. 543 (2012) 185–192. doi:10.1016/J.MSEA.2012.02.073.

[5] O. El Sebaie, A.M. Samuel, F.H. Samuel, H.W. Doty, The effects of mischmetal, cooling rate and heat treatment on the eutectic Si particle characteristics of A319. 1, A356. 2 and A413. 1 Al-Si casting alloys, Mater. Sci. Eng. A, Struct. Mater. Prop. Microstruct. Process. 480 (2008) 342–

355.

[6] Z. Li, N. Limodin, A. Tandjaoui, P. Quaegebeur, J.-F. Witz, D. Balloy, Damage investigation in A319 aluminum alloy by digital image correlation during in-situ tensile tests, Procedia Struct. Integr. 2 (2016) 3415–3422.

[7] Z. Ma, A.M. Samuel, F.H. Samuel, H.W. Doty, S. Valtierra, A study of tensile properties in Al–Si–Cu and Al–Si–Mg alloys: Effect of β-iron intermetallics and porosity, Mater. Sci. Eng. A. 490 (2008) 36–51.

[8] F.H. Samuel, Incipient melting of Al5Mg8Si6Cu2 and Al2Cu intermetallics in unmodified and strontium-modified Al--Si--Cu--Mg (319) alloys during solution heat treatment, J. Mater. Sci. 33 (1998) 2283–2297. doi:10.1023/A:1004383203476.

[9] E. Sjölander, S. Seifeddine, Optimisation of solution treatment of cast Al–Si–Cu alloys, Mater. Des. 31 (2010) S44–S49. doi:10.1016/J.MATDES.2009.10.035.

[10] E. Sjölander, S. Seifeddine, The heat treatment of Al–Si–Cu–Mg casting alloys, J. Mater. Process. Technol. 210 (2010) 1249–1259. doi:10.1016/J.JMATPROTEC.2010.03.020.

[11] P. Ouellet, F.H. Samuel, Effect of Mg on the ageing behaviour of Al-Si-Cu 319 type aluminium casting alloys, J. Mater. Sci. 34 (1999) 4671–4697. doi:10.1023/A:1004645928886.

[12] E. Ogris, A. Wahlen, H. Lüchinger, P.. Uggowitzer, On the silicon spheroidization in Al–Si alloys, J. Light Met. 2 (2002) 263–269. doi:10.1016/S1471-5317(03)00010-5.

[13] L.A. Narayanan, F.H. Samuel, J.E. Gruzleski, Dissolution of iron intermetallics in Al-Si Alloys through nonequilibrium heat treatment, Metall. Mater. Trans. A. 26 (1995) 2161–2174. doi:10.1007/BF02670687.

[14] H. Toda, T. Nishimura, K. Uesugi, Y. Suzuki, M. Kobayashi, Influence of high-temperature solution treatments on mechanical properties of an Al–Si–Cu aluminum alloy, Acta Mater. 58 (2010) 2014–2025.

[15] B. Andilab, C. Ravindran, N. Dogan, A. Lombardi, G. Byczynski, In-situ analysis of incipient melting of Al2Cu in a novel high strength Al-Cu casting alloy using laser scanning confocal microscopy, Mater. Charact. 159 (2020) 110064. doi:https://doi.org/10.1016/j.matchar.2019.110064.

[16] A.M.A. Mohamed, F.H. Samuel, A review on the heat treatment of Al-Si-Cu/Mg casting alloys, in: Heat Treat. Nov. Appl., IntechOpen, 2012.

[17] E. Vandersluis, B. Andilab, C. Ravindran, M. Bamberger, In-situ characterization of the solution heat treatment of B319 aluminum alloy using x-ray diffraction and electron microscopy, Mater. Charact. (2020) 110499.

[18] S. Dezecot, J.-Y. Buffiere, A. Koster, V. Maurel, F. Szmytka, E. Charkaluk, N. Dahdah, A. El Bartali, N. Limodin, J.-F. Witz, In situ 3D characterization of high temperature fatigue damage mechanisms in a cast aluminum alloy using synchrotron X-ray tomography, Scr. Mater. 113 (2016) 254–258. doi:10.1016/J.SCRIPTAMAT.2015.11.017.

[19] L. Lasa, J.M. Rodriguez-Ibabe, Characterization of the dissolution of the Al2Cu phase in two Al–Si–Cu–Mg casting alloys using calorimetry, Mater. Charact. 48 (2002) 371–378. doi:https://doi.org/10.1016/S1044-5803(02)00283-8.

[20] Z. Li, A.M. Samuel, F.H. Samuel, C. Ravindran, S. Valtierra, Effect of alloying elements on the segregation and dissolution of CuAl 2 phase in Al-Si-Cu 319 alloys, J. Mater. Sci. 38 (2003) 1203–1218.

[21] C.M. Dinnis, J.A. Taylor, A.K. Dahle, As-cast morphology of iron-intermetallics in Al-Si foundry alloys, Scr. Mater. 53 (2005) 955–958. doi:10.1016/j.scriptamat.2005.06.028.

[22] C. Puncreobutr, P.D. Lee, R.W. Hamilton, A.B. Phillion, Quantitative 3D Characterization of Solidification Structure and Defect Evolution in Al Alloys, JOM. 64 (2012) 89–95. doi:10.1007/s11837-011-0217-9.

[23] L. Salvo, M. Suéry, A. Marmottant, N. Limodin, D. Bernard, 3D imaging in material science: Application of X-ray tomography, Comptes Rendus Phys. 11 (2010) 641–649. doi:10.1016/J.CRHY.2010.12.003.

[24] Y. Zhao, D. Song, B. Lin, C. Zhang, D. Zheng, S. Inguva, T. Li, Z. Sun, Z. Wang, W. Zhang, 3D characterization of ultrasonic melt processing on the microstructural refinement of AlCu alloys using synchrotron X-ray tomography, Mater. Charact. 153 (2019) 354–365.

[25] D. Kim, J. Kim, E. Kobayashi, Microstructure characterization of rolled Al-Si-Mg-Fe alloy by three-dimensional tomography, Mater. Sci. Eng. A. 768 (2019) 138449. doi:https://doi.org/10.1016/j.msea.2019.138449.

[26] D.L. Lubell, Drawbacks and limitations of computed tomography, Texas Hear. Inst. J. 32 (2005) 250.

[27] J.-Y. Buffiere, E. Maire, J. Adrien, J.-P. Masse, E. Boller, In situ experiments with X ray tomography: an attractive tool for experimental mechanics, Exp. Mech. 50 (2010) 289–305.

[28] Z. Li, N. Limodin, A. Tandjaoui, P. Quaegebeur, J.-F. Witz, D. Balloy, In-situ 3D characterization of tensile damage mechanisms in A319 aluminium alloy using X-ray tomography and digital volume correlation, Mater. Sci. Eng. A. 794 (2020) 139920. doi:https://doi.org/10.1016/j.msea.2020.139920.

[29] B.M. Patterson, J.P. Escobedo-Diaz, D. Dennis-Koller, E. Cerreta, Dimensional quantification of embedded voids or objects in three dimensions using X-ray tomography, Microsc. Microanal. 18 (2012) 390.

[30] A. Velichko, F. Mücklich, Quantitative 3D characterisation of graphite morphology in cast iron–correlation between processing, microstructure and properties, Int. J. Mater. Res. 100 (2009) 1031–1037.

[31] R. Ruxanda, D.M. Stefanescu, Graphite shape characterisation in cast iron—from visual estimation to fractal dimension, Int. J. Cast Met. Res. 14 (2002) 207–216.

[32] W. Aiqin, L. ZHANG, X. Jingpei, Effects of cerium and phosphorus on microstructures and properties of hypereutectic Al-21% Si alloy, J. Rare Earths. 31 (2013) 522–525.

[33] C. Yang, Y. Li, D. Bo, H. Lue, L.I.U. Feng, Effects of cooling rate on solution heat treatment of as-cast A356 alloy, Trans. Nonferrous Met. Soc. China. 25 (2015) 3189–3196.

[34] V. Boulos, V. Fristot, D. Houzet, L. Salvo, P. Lhuissier, Investigating performance variations of an optimized GPU-ported granulometry algorithm, in: Proc. 2012 Conf. Des. Archit. Signal Image Process., IEEE, 2012: pp. 1–6.

[35] N.C.. Kuijpers, J. Tirel, D.. Hanlon, S. van der Zwaag, Quantification of the evolution of the 3D intermetallic structure in a 6005A aluminium alloy during a homogenisation treatment, Mater. Charact. 48 (2002) 379–392. doi:10.1016/S1044-5803(02)00289-9.

[36] C.-L. Chen, A. Richter, R.C. Thomson, Mechanical properties of intermetallic phases in multi-component Al–Si alloys using nanoindentation, Intermetallics. 17 (2009) 634–641. doi:10.1016/J.INTERMET.2009.02.003.

[37] Z. Li, N. Limodin, A. Tandjaoui, P. Quaegebeur, J.F. Witz, D. Balloy, Influence of Fe content on the damage mechanism in A319 aluminum alloy: Tensile tests and digital image correlation, Eng. Fract. Mech. 183 (2017) 94–108. doi:10.1016/j.engfracmech.2017.05.006.

[38] K. Du, Q. Zhu, D. Li, F. Zhang, Study of formation mechanism of incipient melting in thixo-cast Al–Si–Cu–Mg alloys, Mater. Charact. 106 (2015) 134–140.

[39] C. Zhang, Z. Cai, R. Wang, C. Peng, Y. Feng, Enhancing densification capacity and properties

of Al/diamond composites by partial liquid hot pressing, Surf. Coatings Technol. 313 (2017) 347–354.

[40] S. Lippmann, C. Simon, S. Zechel, M. Seyring, U.S. Schubert, G. Wilde, M. Rettenmayr, Determining solid/liquid interfacial energies in Al-Cu by curvature controlled melting point depression, Acta Mater. 147 (2018) 113–121.

[41] M. Tash, F.H. Samuel, F. Mucciardi, H.W. Doty, Effect of metallurgical parameters on the hardness and microstructural characterization of as-cast and heat-treated 356 and 319 aluminum alloys, Mater. Sci. Eng. A. 443 (2007) 185–201.

[42] P.-S. Wang, S.-L. Lee, J.-C. Lin, M.-T. Jahn, Effects of solution temperature on mechanical properties of 319.0 aluminum casting alloys containing trace beryllium, J. Mater. Res. 15 (2000) 2027–2035.

[43] M.A. Moustafa, F.H. Samuel, H.W. Doty, Effect of solution heat treatment and additives on the microstructure of Al-Si (A413. 1) automotive alloys, J. Mater. Sci. 38 (2003) 4507–4522.

[44] M.A. Moustafa, F.H. Samuel, H.W. Doty, Effect of solution heat treatment and additives on the hardness, tensile properties and fracture behaviour of Al-Si (A413. 1) automotive alloys, J. Mater. Sci. 38 (2003) 4523–4534.

[45] S.A. Al Kahtani, H.W. Doty, F.H. Samuel, Combined effect of melt thermal treatment and solution heat treatment on eutectic Si particles in cast Al–Si alloys, Int. J. Cast Met. Res. 27 (2014) 38–48.

[46] I. Sadeghi, M.A. Wells, S. Esmaeili, Effect of particle shape and size distribution on the dissolution behavior of Al2Cu particles during homogenization in aluminum casting alloy Al-Si-Cu-Mg, J. Mater. Process. Technol. 251 (2018) 232–240.

[47] H.B. Aaron, On the kinetics of precipitate dissolution, Met. Sci. J. 2 (1968) 192–193.

[48] M.J. Whelan, On the kinetics of precipitate dissolution, Met. Sci. J. 3 (1969) 95–97.

[49] L.C. Brown, Diffusion-controlled dissolution of planar, cylindrical, and spherical precipitates, J. Appl. Phys. 47 (1976) 449–458.

[50] A.K. Kulshreshtha, O.N. Singh, G.M. Wall, Pharmaceutical suspensions: from formulation development to manufacturing, Springer, 2009.

[51] I.M. Lifshitz, V.V. Slyozov, The kinetics of precipitation from supersaturated solid solutions, J. Phys. Chem. Solids. 19 (1961) 35–50. doi:10.1016/0022-3697(61)90054-3.

[52] WAGNER, C., Theory of Precipitate Change by Redissolution, Z. Elektrochem. 65 (1961) 581–591. http://ci.nii.ac.jp/naid/10030120881/en/ (accessed 16 March 2019).

[53] O. Reiso, H.-G. Øverlie, N. Ryum, Dissolution and melting of secondary Al 2 Cu phase particles in an AlCu alloy, Metall. Trans. A. 21 (1990) 1689–1695.

[54] N. Crowell, S. Shivkumar, Solution Treatment Effects in Cast Al-Si-Cu Alloys (95-107), Trans. Am. Foundrymen's Soc. 103 (1995) 721–726.